Available online at www.sciencedirect.com
SCIENCE DIRECT®
Journal of Sound and Vibration 281 (2005) 483–507
JOURNAL OF SOUND AND VIBRATION
www.elsevier.com/locate/jsvi

Wave motion in thin-walled structures

L. Houillon[a], M.N. Ichchou[b,*], L. Jezequel[b]

[a]*Peugeot Citroen DTAT/DMTC/MTS, Route de Gisy, 78943 Velizy, Villacoublay, France*
[b]*Laboratoire de Mécanique des Solides, Département de Mécanique des Solides, Génie Mécanique et Génie Civil École Centrale de Lyon, 36, Avenue Guy de Collongues, BP 163, 69131 Ecully, France*

Received 24 May 2002; accepted 27 January 2004
Available online 13 October 2004

Abstract

The characterization of propagation constants of realistic thin-walled structures with any cross-section is studied in this paper. A propagative approach is proposed in order to extract propagation parameters. Specifically, by using an existing finite element model, the formulation provides an effective way to calculate the dispersion curves of realistic thin-walled structures. Some numerical results are presented to show that the described method can be applied to simple laboratory structures (cylinders, plate box structures) and typical automotive hollow structures.

1. Introduction

The structural energy transferring through hollow structures is of great interest in many areas of mechanical engineering such as the automotive industry. Indeed, such components play a leading role in the energy transfer paths from the engine sources to panels, creating sound radiation and unwanted vibration leading to fatigue, and associated structural borne sound phenomenon. Mastering the dynamical behaviour of hollow structures can provide an efficient and physically satisfactory means to passively optimize the car chassis.

*Corresponding author. Tel.: +33-04-72-18-62-30; fax: +33-04-72-18-91-44.
E-mail address: ichchou@mecasola.ec-lyon.fr (M.N. Ichchou).

0022-460X/$ - see front matter © 2004 Elsevier Ltd. All rights reserved.
doi:10.1016/j.jsv.2004.01.020

However, achieving such a lofty objective may differ by virtue of the optimization context. For instance, at preliminary stages of product life, one mainly needs optimization tools capable of providing global tendencies rapidly. Such optimization tools will also depend on the frequency range in question. Indeed, the situation will be different if low-frequency dynamics or high-frequency behaviour are considered. In this paper, the authors pursue two main objectives: (1) provide physical parameters of considered structures, enabling a pertinent analysis of disturbance paths; (2) provide inputs for low-frequency as well as high-frequency prediction tools.

A wave description of the concerned phenomenon facilitates approaches to both the required objectives [1,2]. Indeed, from the knowledge of wave content, one can imagine some interesting optimization solutions. For instance, from the geometrical and mechanical properties of the structures, one can control waves carrying most of the energy or generating excessive sound. Moreover, mastering free waves can be used in order to provide forced dynamics for a wide class of vibroacoustical problems. In fact, the latter will provide a new set of functions and basis. This is an alternative to the well-known finite element methods (FEM) [3]. Accordingly, use of wave content will enable avoidance of FEM limitations mainly at medium and high frequencies. In addition, if the latter frequency range is considered, the corresponding prediction tools can take advantage of a free wave analysis.

Specifically, if energy-predictive tools are considered (among them are the well-known predictive *statistical energy analysis* (SEA) [4–7] and its local energy formats [8–12]), the main predictive analysis requires wave characteristics to be known. Indeed, most of the predictive energy methods need energy transmission coefficients, energy velocities and modal densities to be given [13]. Generally, the latter are obtained from simplified theories (beams, plates, shells, acoustic media, etc.). However, analytical models often originate from approximate theories (in terms of strain and stress tensors format) and some of them are of limited interest particularly at high frequencies, while intuitively full 3D models seem to be required. One of the major contributions of this paper is to provide a numerical tool in order to study such structural complexity. Indeed, this numerical wave extraction approach, based on the use of existing finite element models, will notably improve subsystem definitions. This is, in a sense, a *hybridization between FEM and SEA or other techniques*.

Referring to the existing literatures, dispersion curve extraction techniques through hybridization with a finite element code is not something completely new. Indeed many authors have been interested in a numerical determination of dispersion curves for particular structures. Among those contributors, the work of Gavric [14,15] and the contribution of Knothe [16] should be noted. Gavric and Knothe applied this extraction technique for rail structures. This engineering field seems to be the precursor. Indeed, the size of rail structures allows a dynamical motion synthesis from a free wave study. In Refs. [14,15], Gavric proposed a particular finite element scheme allowing the extraction of wavenumbers from the resolution of a four-order matrix equation. In Ref. [16], Knothe introduced a numerical scheme well suited to infinite rail structures. The use of the latter allows dispersion curve extraction from a well-posed eigenproblem. However, both Gavric and Knothe run into some numerical difficulties. Indeed, the first technique requires the development of a relatively new finite element code with specific elements, interpolation forms and an adapted eigenvalue extraction method. As for the second method, the structures are designated by an infinite succession of identical hyperelements, so that

the cross-sections of each side are the same and the resulting mesh has internal nodes. This leads to a complex computational problem.

Some interesting work on the problem at hand can be found in the literature on periodic structures and systems. Among them is Lin's work [17]. Lin proposed in Ref. [17] a procedure for using the transfer matrix concept, in which beam-like structures as well as curved panel examples were examined. This method runs into difficulties due to the inversion of ill-conditioned matrices and the cumulative errors due to the transfer matrix assembly. Mead [18,19] introduced fundamental and central ideas in the area of periodic systems characterization. In this context, Mead proposed in Ref. [18] a quadratic and well-posed spectral problem in order to determine wave propagation constants of a periodic system. This work was extended in Refs. [19,20], Denke et al. [20] and Mead [19] proposed a second-order matrix equation leading to the propagation constants of a periodic system. Thompson [21] used the same technique after adding a damping contribution. Finally, the interesting work by Zhong et al. [22,23] should be mentioned. Zhong [22] offered a new eigenvalue problem, which is a kind of state space eigenproblem, wherein the main parameters are the displacements at both sections of the considered system.

To the author's knowledge, applications of numerical dispersion curve extraction techniques in the field of vibroacoustic were suggested recently by Finnveden [24,25], and by Ichchou [26]. Finnveden proposed the so-called spectral FEM, whose objectives are very close to the propagative approach [27,28] called by authors. In fact, both approaches tend to give the dispersion curves of typical dynamical systems and related forced responses. Orrenius and Finnveden presented applications of this concept for extended stiffened plates [29] and for pipeworks [25]. A number of applications are given in Refs. [27,30–32] for elastoacoustic and periodic structures. Here, hollow structures are considered [28,33].

In this contribution, a dispersion curve extraction technique whose principal feature is to be quickly integrated in any existing finite element code is proposed, trying also to avoid the previously explained drawbacks of the other methods. To start, the finite element model of any cross-section topology of a thin-walled structure is proposed. This is a classical representation of the general equations of motion. The main feature, which is linked to the thin-walled propagation characteristic, is thus introduced. Combining the proposed propagation law and an equivalent finite element model allows an eigenvalue problem to be written. The properties of such an eigenvalue problem are first discussed. Numerical implementation under a FEM code of the resulting spectral problem is thoroughly discussed in Section 3. This leads to a simple tool able to deal with any topology of a thin-walled structure being studied. Sections 4 and 5 are mainly devoted to the validation of the numerical procedure proposed. In Section 4, the formulation is compared with analytical theories for academic thin-walled structures. Two examples are given. The first is a simple cylinder whose behaviour is well referenced in the literature [34]. The second example, is an extended plate box structure with no immediate simplified theory available in the literature. An approximate plate assembly theory is proposed in this paper and compared to the numerical extraction technique. Finally, Section 5 proposes a validation of the method on a realistic automotive structure as well as a parametric study in order to examine the wave grasp of practical structures.

2. Dispersion curve computation

In this work, thin-walled structures are assimilated to a complex waveguide. To simplify the following developments, a linear elastic, homogenous solid is considered. No damping is added here in order to facilitate the numerical integration in a FEM code. In the following, the main assumption used, traducing the waveguide property is

$$u_i = U_i e^{-jkx} e^{j\omega t}, \tag{1}$$

u_i being any kinematic field. Eq. (1) states a harmonic dependency of the primary structural forces with respect to the main axis of propagation, namely x below. The time dependency states a pure steady-state context. Indeed, no transient analysis will be performed in this text. In view of the wave extraction technique used in this study, the FEM modelling of the structure will be briefly explained. The aim here is to reuse FEM matrixes and to prepare the post-processing of data. Thus, the extraction procedure and its properties will be explained and discussed.

2.1. Finite element description

Unlike the Gavric extraction technique [14], the procedure used here relies on an existing FEM model of the problem. This procedure uses simple 2D meshing of a section of the thin-walled structure. For the computation need, the meshing is extended by a length d: which indirectly amounts to meshing a piece of structure that contains no intermediate nodes between the left and right sections (see Fig. 1). The latter is the principal difference with the Knothe [16] procedure in which a full meshing of the elementary section is defined. l and r designate the parameters and quantities corresponding to the left cross-section and the right cross-section with respect to the x-axis. In order to take into account different motion types in the hollow structure, four degrees of freedom are attached to each node: three translations and the rotation around the x-axis. A finite element description of such a problem allows characterization of the structural dynamics. The following notations and definitions will be used below:

$$[U] = \begin{bmatrix} U_l \\ U_r \end{bmatrix}, \quad [F] = \begin{bmatrix} F_l \\ F_r \end{bmatrix}, \tag{2}$$

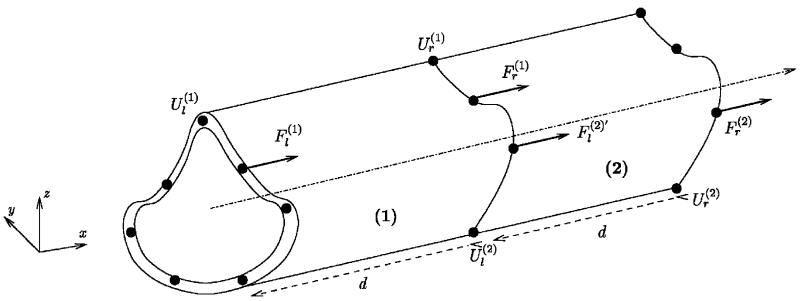

Fig. 1. Typical thin-walled structure.

$[U]$ and $[F]$ being, respectively, the nodal displacement and forces.

$$[\mathbf{K}] = \begin{bmatrix} \mathbf{K}_{ll} & \mathbf{K}_{lr} \\ \mathbf{K}_{rl} & \mathbf{K}_{rr} \end{bmatrix}, \quad [\mathbf{M}] = \begin{bmatrix} \mathbf{M}_{ll} & \mathbf{M}_{lr} \\ \mathbf{M}_{rl} & \mathbf{M}_{rr} \end{bmatrix}, \tag{3}$$

where $[\mathbf{K}]$ and $[\mathbf{M}]$ are the partitioned stiffness and mass matrices. With $[\mathbf{K}_{rl}] = [\mathbf{K}_{lr}]^t$ and $[\mathbf{M}_{rl}] = [\mathbf{M}_{lr}]^t$, as far as conservative systems are concerned here, mass and stiffness matrices are symmetrical. The finite element representation from matrix knowledge leads to

$$\begin{bmatrix} \mathbf{S}_{ll} & \mathbf{S}_{lr} \\ \mathbf{S}_{rl} & \mathbf{S}_{rr} \end{bmatrix} \begin{bmatrix} U_l \\ U_r \end{bmatrix} = \begin{bmatrix} F_l \\ F_r \end{bmatrix} \tag{4}$$

with $\mathbf{S}_{ij} = \mathbf{K}_{ij} - \omega^2 \mathbf{M}_{ij}$; $\forall i,j \in \{l,r\}$. Introducing the relationship $F'_l = -F_l$ produces the new system of equations (5), where F'_l and F_r have the same sense.

$$\begin{bmatrix} -\mathbf{S}_{ll} & -\mathbf{S}_{lr} \\ \mathbf{S}_{rl} & \mathbf{S}_{rr} \end{bmatrix} \begin{bmatrix} U_l \\ U_r \end{bmatrix} = \begin{bmatrix} F'_l \\ F_r \end{bmatrix}. \tag{5}$$

This is a well-established equation, which can be reached from any finite element code. The only additional operation required consists of partitioning the resulting matrices and vectors with respect to the main propagation axis.

2.2. Waveguide assumption

The resulting system of equations (5) is classical in a finite element description of structures. However, this equation does not take into account the physical aspect of the model. Indeed, the waveguide assumption represented in Eq. (1) must be integrated. In the following work, this formula will be introduced by means of the term $\lambda = \mathrm{e}^{-\mathrm{j}kd}$ (k being the wavenumber and d the modelling length considered). This assumption results in the following expression (6):

$$U_r = \lambda U_l. \tag{6}$$

Fig. 1 examines two adjacent identical elementary sections of the considered thin-walled structure, designated, respectively, by parts (1) and (2). The fact that parts (1) and (2) are considered identical, produces an identical, mass and stiffness matrix so that

$$\mathbf{S}_{ij}^{(1)} = \mathbf{S}_{ij}^{(2)}, \quad \forall i,j \in \{l,r\}. \tag{7}$$

Eqs. (5) and (7) lead to the following expression:

$$\begin{bmatrix} -\mathbf{S}_{ll} & -\mathbf{S}_{lr} \\ \mathbf{S}_{rl} & \mathbf{S}_{rr} \end{bmatrix} \begin{bmatrix} U_l^{(1)} \\ U_r^{(1)} \end{bmatrix} = \begin{bmatrix} F_l'^{(1)} \\ F_r^{(1)} \end{bmatrix}, \quad \begin{bmatrix} -\mathbf{S}_{ll} & -\mathbf{S}_{lr} \\ \mathbf{S}_{rl} & \mathbf{S}_{rr} \end{bmatrix} \begin{bmatrix} U_l^{(2)} \\ U_r^{(2)} \end{bmatrix} = \begin{bmatrix} Fc_l'^{(2)} \\ F_r^{(2)} \end{bmatrix}.$$

So,

$$F_l'^{(2)} = -\mathbf{S}_{ll} U_l^{(2)} - \mathbf{S}_{lr} U_r^{(2)}, \tag{8}$$

or equivalently,

$$F_l'^{(2)} = -\mathbf{S}_{ll} U_l^{(2)} - \lambda \mathbf{S}_{lr} U_l^{(2)}. \tag{9}$$

At the interface between both sections, displacement continuity ($U_r^{(1)} = U_l^{(2)}$) as well as equilibrium forces ($F_l'^{(2)} = F_r^{(1)}$) lead to

$$F_r^{(1)} = -\mathbf{S}_{ll} U_r^{(1)} - \lambda \mathbf{S}_{lr} U_r^{(1)}. \tag{10}$$

This expression can be put in another format:

$$F_r^{(1)} = -\lambda \mathbf{S}_{ll} U_l^{(1)} - \lambda \mathbf{S}_{lr} U_r^{(1)}, \tag{11}$$

which induces an effort proportionality expression, namely

$$F_r^{(1)} = \lambda F_l'^{(1)}. \tag{12}$$

Expressions (6) and (12) allow an eigenvalue problem to be proposed. The latter is given in the next subsection.

2.3. Eigenvalue problem

Putting the respective expressions of U_r and F_r, namely expressions (6) and (12), into the system equation (5), leads to an eigenvalue problem:

$$\begin{bmatrix} -\mathbf{S}_{ll} & -\mathbf{S}_{lr} \\ \mathbf{S}_{rl} & \mathbf{S}_{rr} \end{bmatrix} \begin{bmatrix} U_l \\ \lambda U_l \end{bmatrix} = \begin{bmatrix} F_l' \\ \lambda F_l' \end{bmatrix}. \tag{13}$$

Eliminating F_l' from this expression allows expression (13) to be written in the more convenient format as follows:

$$\left(\mathbf{S}_{rl} + \lambda(\mathbf{S}_{ll} + \mathbf{S}_{rr}) + \lambda^2 \mathbf{S}_{lr}\right) U_l = 0. \tag{14}$$

This eigenvalue problem allows numerical determination of eigenvalues (λ_i) as well as eigenvectors U_{li}. Obviously, from the U_{li} expression, one can readily establish the remaining displacement and force quantities. Expression (14) is close to the spectral problem proposed by Denke et al. [20] and by Mead in Ref. [18]. Thompson in Ref. [21] used this equation in order to extract a dispersion curve for rail structures. This eigenvalue problem will not be implemented as it is proposed in expression (14). A modified format is proposed in the next subsection.

2.4. Computed eigenvalues and basic properties

As discussed previously, Eq. (14) is sufficient to establish the dispersion curve extraction using a finite element model of thin-walled structure. However, in order to avoid some of the numerical difficulties arising from the non-standard format of such an equation, the latter will be put in a more convenient format (numerically speaking). But, first, some remarks based on an immediate examination of expression (14) can be drawn:

- If the mass and stiffness matrix dimension is (n, n), Eq. (14) admits $2n$ eigenvalues.
- If λ is an eigenvalue, then $1/\lambda$ is an eigenvalue stating a reciprocity in the propagation mechanism.

Eq. (14) is not used directly for the computation of dispersion curves. This equation can be modified using a state space representation of the problem. Indeed, system (14) can be put in the following simple format:

$$\begin{bmatrix} -\mathbf{S}_{ll} & -\mathbf{I} \\ \mathbf{S}_{rl} & \mathbf{O} \end{bmatrix} \begin{bmatrix} U_l \\ F'_l \end{bmatrix} = \begin{bmatrix} \mathbf{S}_{lr} & \mathbf{O} \\ -\mathbf{S}_{rr} & \mathbf{I} \end{bmatrix} \begin{bmatrix} U_r \\ F_r \end{bmatrix}. \tag{15}$$

The use of a state space representation is an interesting alternative to the spectral analysis which must be performed in the context of numerical dispersion curve extraction. A more detailed study on the subject is proposed in Refs. [32,27]. Such a formulation was also used by Zhong in Ref. [23]. Eq. (15) when combined with expressions (6) and (11) can lead to an eigenvalue problem, which can be solved by standard numerical eigensolution extraction. In this contribution, another alternative is proposed. Indeed, from expression (15), it can be readily established that

$$\begin{bmatrix} -\mathbf{S}_{lr}^{-1}\mathbf{S}_{ll} & -\mathbf{S}_{lr}^{-1} \\ \mathbf{S}_{rl} - \mathbf{S}_{rr}\mathbf{S}_{lr}^{-1}\mathbf{S}_{ll} & -\mathbf{S}_{rr}\mathbf{S}_{lr}^{-1} \end{bmatrix} \begin{bmatrix} U_l \\ F'_l \end{bmatrix} = \begin{bmatrix} U_r \\ F_r \end{bmatrix}. \tag{16}$$

Combining the propagation expressions ($U_r = \lambda U_l$) and ($F_r = \lambda F'_l$), a new system of equations can be written:

$$(\mathbf{N} - \lambda \mathbf{I}_2)u = 0, \tag{17}$$

with

$$u = \begin{bmatrix} U_l \\ U_r \end{bmatrix} \tag{18}$$

and

$$\mathbf{N} = \begin{bmatrix} -\mathbf{S}_{lr}^{-1}\mathbf{S}_{ll} & -\mathbf{S}_{lr}^{-1} \\ \mathbf{S}_{rl} - \mathbf{S}_{rr}\mathbf{S}_{lr}^{-1}\mathbf{S}_{ll} & -\mathbf{S}_{rr}\mathbf{S}_{lr}^{-1} \end{bmatrix}, \tag{19}$$

$\mathbf{I}_2$ being a $(2n, 2n)$ identity matrix. Introducing matrix $\mathbf{J}$ which is a particular matrix defined by

$$\mathbf{J} = \begin{bmatrix} \mathbf{O} & \mathbf{I} \\ -\mathbf{I} & \mathbf{O} \end{bmatrix}. \tag{20}$$

It can be readily shown that matrices $\mathbf{N}$ and $\mathbf{J}$ verify

$${}^t\mathbf{N}\mathbf{J}\mathbf{N} = \mathbf{J}, \tag{21}$$

$\mathbf{N}$ being a symplectic matrix. Expression (21) comes mainly from the following relationships:

$${}^t\mathbf{S}_{ll} = \mathbf{S}_{ll}, \quad {}^t\mathbf{S}_{rr} = \mathbf{S}_{rr}, \quad {}^t\mathbf{S}_{rl}^{-1} = \mathbf{S}_{lr}^{-1}. \tag{22}$$

Multiplying Eq. (17) by ${}^t\mathbf{N}\mathbf{J}$ and using the symplectic property of matrix $\mathbf{N}$, the system (17) becomes

$$\mathbf{J}u = \lambda {}^t\mathbf{N}\mathbf{J}u, \tag{23}$$

where

$$u = \begin{bmatrix} U_l \\ F'_l \end{bmatrix}. \tag{24}$$

Dividing by λ (non-null term) and after transposing the expression,

$${}^t(\mathbf{J}u)(\mathbf{N} - \lambda^{-1}\mathbf{I}_2) = 0. \tag{25}$$

Equality expression (25) proves once again that $1/\lambda$ is equally an eigenvalue of the system (17), with ${}^t(\mathbf{J}u)$ as an eigenvector. Ultimately, as $\mathbf{S}_{ij}$ are frequency dependent, the resulting spectral problem must be solved at each frequency step. Henceforth, wavenumbers (or energy velocities reached here using a centred finite difference scheme) can be obtained at each frequency and therefore eigenvectors. The latter will play a dominant role in the propagation branch explanation. Drawing eigenvectors versus frequency will allow meticulous identification of motion of the thin-walled structure. This procedure was implemented in order to enable the analysis of any topology of thin-walled structures.

3. Implementation of the propagative approach

3.1. Preparation of data

The first step in the implementation procedure is the extraction of a finite element model of the studied thin-walled structure. The following parameters are thus needed:

- the propagation distance d;
- initial frequency of analysis;
- frequency increment;
- number of frequency steps under consideration;
- selection criterion ε.

As far as thin-walled structures are concerned, the propagation distance d is chosen here so that the thin shell theory is satisfied. Practically, propagation distance d is kept approximately equal to the average internodal distance for the left generated section. The frequency range in which the dispersion curve extraction is needed can be chosen almost arbitrarily. However, as the spectral analysis is done at each frequency step, the number of steps must be kept to a reasonable number. At each frequency step, the generated FEM job is numerically processed in order to determine eigensolutions. The eigenvalue extraction tool chosen here is the complex biorthogonal Lanczos method. It is known, among the existing eigenvalue extraction tools (Hessenberg method, inverse power method), for its good convergence. Eigenvalues λ_i ($\lambda_i = \mathrm{e}^{-\mathrm{j}k_i d}$) are thus extracted at each frequency step, allowing the corresponding wavenumbers k_i to be identified. The extracted wavenumbers can be either real, pure imaginary or complex. The parameter ε introduced previously allows classification of propagation constants. In practice, the selection is established according to the following:

- k is real if $|\mathrm{Im}(k)| < \varepsilon$;

- k is pure imaginary if $|\mathrm{Re}(k)| < \varepsilon$;
- k is complex if $|\mathrm{Re}(k)| > \varepsilon$ and $|\mathrm{Im}(k)| > \varepsilon$.

This procedure is achieved at each frequency step, time consumption will be mainly linked to the structural complexity of the thin-walled structure, to the size of matrices and to the frequency band and step under consideration.

3.2. Processing of eigensolutions

The last step in the implementation procedure consists of presenting the dispersion curve. Precisely, post-processing of the results from the previous section allows the dispersion curve, namely, $k = f(\omega)$ to be drawn as well as the display of the eigenvectors, representing the sectional modes for each frequency. Indeed, to draw the dispersion curves from the given eigenvalues at each frequency step, a discrete procedure is employed in order to check the coherence of the resulting propagation branches. In this contribution, a MAC number is employed. In fact, two complex eigenvectors u and v associated with two distinct eigenvalues can be expressed as follows:

$$\mathrm{MAC}(u, v) = \frac{({}^t u \cdot \overline{v})({}^t v \cdot \overline{u})}{({}^t u \cdot \overline{u})^2 ({}^t v \cdot \overline{v})^2}. \tag{26}$$

Two eigenvectors calculated at two consecutive steps correspond to the same eigenvalue if the MAC number is close to the unity. Such a criterion is easy to implement and does not affect the CPU consumption of the extraction procedure. It easily allows the propagation branches to be plotted coherently. This procedure also allows the cut-on frequencies to be identified efficiently.

At this stage, the implementation procedure is completed. It leads to a simple tool capable of dealing with any kind of topology of thin-walled homogenous structures. In the following section, this tool is employed in order to compare with some analytical results.

4. Validation by comparison with analytical models

The main goal of the present section is to provide some comparisons, in view of the achieved code validations, with some analytical results. For this purpose, two topology sections were chosen. The first one is simply the cylindrical shell geometry. The second validation example chosen is a plate box assembly (an extended beam with rectangular section). In both cases, some analytical results were compared to the numerical extraction procedure detailed previously.

4.1. Cylinders

In this first comparison test, a pure cylindrical shell is considered. Many mechanical models can be adopted in order to deal with the structural borne sound of such structure. Specifically, this structure can be considered as a simple Euler–Bernoulli beam, with flexion as well as traction and torsion motion. Further models were proposed for vibration of cylinders. Among them is the Donnell–Mushtari theory, the Flugge theory, and so on. A more concise study of the mechanics

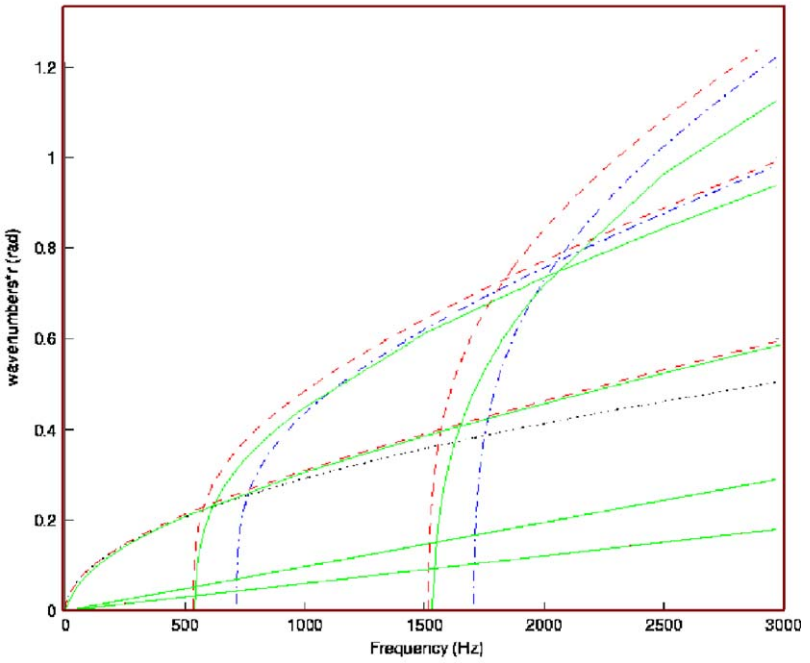

Fig. 2. Comparison of dispersion curves from different theories for cylinders: dotted, Euler–Bernoulli; dashed, Flugge; dash–dot, Donnell–Mushtari; solid, present.

of vibrations of cylindrical shells was provided in Ref. [34]. Donnell–Mushtari's as well as Flugge's theory for cylindrical motion used here were extracted from the latter.

Here, the last three possible models (Euler, Donnel and Flugge) were compared with the results given numerically by the previously exposed method. The numerical test was done using the following mechanical and geometrical considerations: radius $r = 50\,\text{mm}$, thickness $h = 2\,\text{mm}$ and steel material constants ($\rho = 7800\,\text{kg/m}^3$, $\nu = 0.3$ and $E = 21 \times 10^{10}\,\text{Pa}$). From Fig. 2, it can be shown that there is a good correspondence of the low-frequency propagation branches. All of the employed theories predict correctly the flexural, the compressional as well as the torsional branches. Moreover, the cut-on frequencies corresponding to cross-section intrinsic deformation are well predicted by the propagation approach equation (17) when compared with the often employed Flugge cylindrical motion model. Some discrepancies concerning the cut-on frequencies of the Donnell–Mushtari and the Flugge or the propagation approach are mainly due to the deformation assumptions employed in the context of the Donnell–Mushtari model, which is obviously an approximate theory. In addition, when comparing the analytical approximate theories with the numerical approach used here (Eq. (17)), some dissimilarities appear as the frequency increases. Indeed, as it can be seen in Fig. 2, differences between the predicted wavenumber amplitudes predicted increase in high frequencies when comparing the analytical approaches to the numerical technique employed here. This is a predictable result, which is mainly related to the approximate nature of these theories.

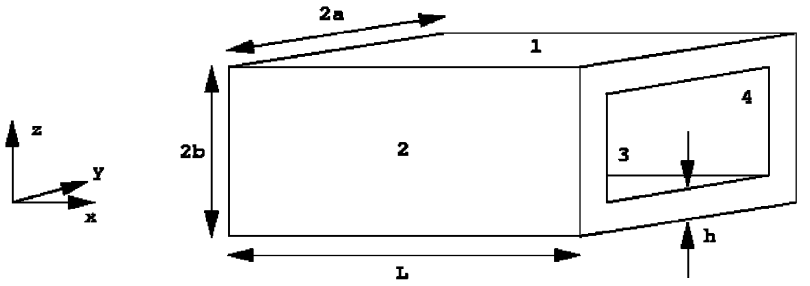

Fig. 3. Plate assembly structure.

4.2. Rectangular plate box thin-walled structure

Here, an aluminium ($\rho = 2700\,\mathrm{kg/m^3}$, $v = 0.33$ and $E = 7.1 \times 10^{10}\,\mathrm{Pa}$) plate box structure is considered. Fig. 3 presents such a structure. Despite its simplicity, no immediate structural theory is proposed in order to deal with its wave motion. For the numerical simulations below, the following values were considered:

$$a = 50\,\mathrm{mm}, \quad b = 25\,\mathrm{mm}, \quad h = 4\,\mathrm{mm}.$$

Here, the section inertia is given by $I = \frac{4}{3}(ba^3 - (b-h)(a-h)^3)$ and $S = 4h(a+b)$ cross-section. As in the previous case, two approximate theories are considered. The first one is the classical Euler beam theory, giving wavenumbers of flexural and extensional waves as follows:

$$k_f = \left(\frac{\omega^2 \rho S}{EI}\right)^{1/4} \quad \text{and} \quad k_t = \omega\left(\frac{\rho}{E}\right)^{1/2}.$$

The second approximate theory introduced here states a particular kinematic for the plate box structure. It should be noted that the choice of such a structure is mainly motivated by the lack of pertinent analytical models or theories to address its dynamical motion. Indeed, this relatively simple structure can be either approximated by a beam theory or discretized using thin plate theory. In this contribution, a third alternative derived from the use of the propagative approach is proposed.

4.2.1. Numerical propagation constant extraction

The numerical extraction procedure is performed first. In this context, from a finite element model of the plate box structure, the propagation constant is derived from such a procedure. Results from the FEM processor are presented in Fig. 4. The frequency range of analysis was fixed at [0–6000 Hz] with a frequency span of 60 Hz. The finite element model comprises five similar *cquad*4 elements per plate.

Fig. 4 presents seven propagation branches in the dispersion curve. These propagation branches correspond to the intrinsic motion of the structure. In order to better understand the nature of each propagation constant, the corresponding eigenvectors were plotted in the frequency domain. This is done for instance in Fig. 5, where the branch number 6 is analysed. The figure clearly indicates the physical nature of each propagation branch. Propagation branches 1–4 describe

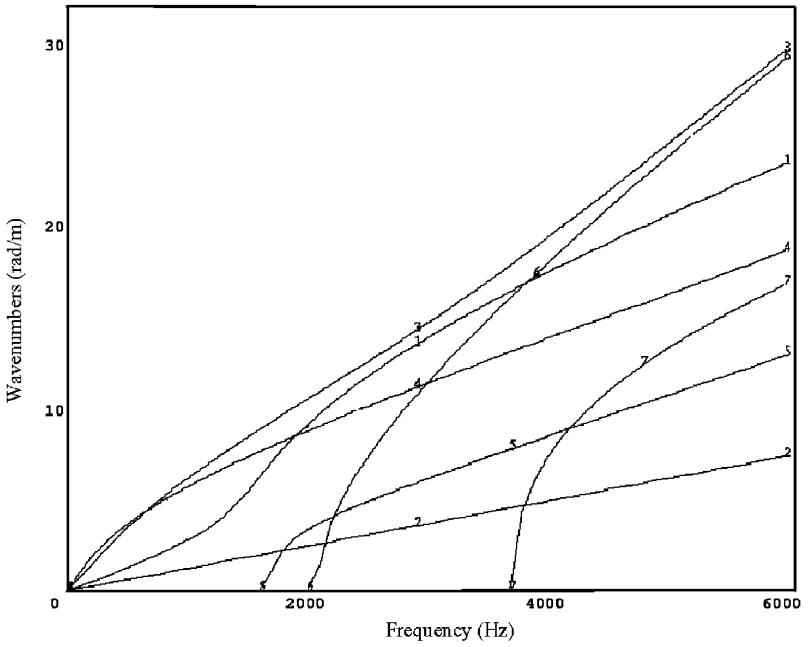

Fig. 4. Numerical computed dispersion curve: (1) torsion; (2) compression; (3) flexion (z); (4) flexion (y); (5) sectional mode—torsion; (6) pumping; (7) sectional mode—flexion.

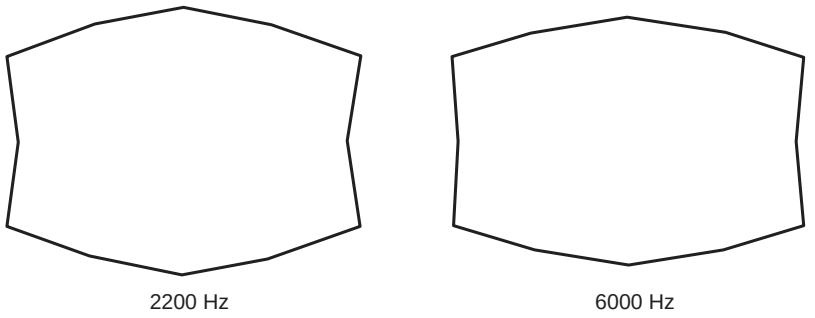

Fig. 5. Frequency evolution of eigenvectors associated to branch wavenumber 6.

classical flexural (in-plane and out-of-plane flexural motion as well), torsional and extensional waves. Branches 5–7 describe, respectively, cross-section torsion, pumping and flexion.

4.2.2. Simplified analytical theory

As mentioned in the previous subsection, analytical theories for any cross-section topology are not easily found. As regards the structural complexity and the concerned frequency range, a 3D elastic model can be used but requires a relatively high numerical cost. In the following, an analytical model is proposed in order to take into account a particular cross-section deformation.

The thin-walled structure is assumed to be a four-plate assembly system. The dispersion curve will be extracted analytically using Hamilton's principle. To do so, consider the waveguide

assumption associated with the propagation along the x-axis and expressing the displacement fields of each plate as follows:

$$\begin{pmatrix} u_i \\ v_i \\ w_i \end{pmatrix} = \begin{pmatrix} U_i(y,z) \\ V_i(y,z) \\ W_i(y,z) \end{pmatrix} \mathrm{e}^{\mathrm{j}kx} \mathrm{e}^{-\mathrm{j}\omega t}, \tag{27}$$

where i is the index of the considered plate, $i = 1, 4$. The kinetic energy associated with the plate assembly system can be readily expressed by

$$T = L \sum_i \int_{S_i} \frac{\rho\omega^2}{2} (\overline{u_i} u_i + \overline{v_i} v_i + \overline{w_i} w_i) \, \mathrm{d}y_i \mathrm{d}z_i, \tag{28}$$

where $\overline{u_i}$ is the complex quantity associated with u_i and S_i is the cross-section of each panel. L is the length of the considered element. Taking into account respective expressions of u_i, v_i and w_i leads to

$$Ec = L \sum_i \int_{S_i} \frac{\rho\omega^2}{2} (\overline{U_i} U_i + \overline{V_i} V_i + \overline{W_i} W_i) \, \mathrm{d}y_i \mathrm{d}z_i. \tag{29}$$

The potential energy expression from the stress and strain tensors can be expressed by

$$Ep = \sum_i \int_{S_i} [\overline{\sigma_i}]^t [\varepsilon_i] \, \mathrm{d}S_i, \tag{30}$$

where $[\sigma_i]$ and $[\varepsilon_i]$ are, respectively, the strain and stress tensors associated with each panel $i = 1, 4$. The strain and stress tensors considered here obey the classical Kirchhoff assumption. Detailed expression of the strain tensor as well as expressions of the stress tensor are given in the following expressions:

$$[\varepsilon_i]^t = \left[\frac{\partial u_i}{\partial x} \; \frac{\partial v_i}{\partial y} \; \frac{\partial u_i}{\partial y} + \frac{\partial v_i}{\partial x} \; \frac{\partial^2 w_i}{\partial x^2} \; \frac{\partial^2 w_i}{\partial y^2} \; 2 \frac{\partial^2 w_i}{\partial x \partial y} \right]^t \tag{31}$$

and

$$[\sigma_i] = \frac{E}{1 - v^2} \begin{bmatrix} h[\mathbf{D}_0] & [\mathbf{O}]_{3\times 3} \\ [\mathbf{O}]_{3\times 3} & \dfrac{h^3}{12}[\mathbf{D}_0] \end{bmatrix} [\varepsilon_i], \tag{32}$$

where

$$[\mathbf{D}_0] = \begin{bmatrix} 1 & v & 0 \\ v & 1 & 0 \\ 0 & 0 & \dfrac{1 - v}{2} \end{bmatrix}. \tag{33}$$

Detailed expressions of the potential energies are given in Appendix A. At this stage, an approximate displacement field may be chosen. The latter may lead to an approximate theory relative to the motion of the plate box structure. The choice of such an approximate displacement field comes from the eigenvector representation. For the sake of analytical simplicity, the so-called *pumping* mode

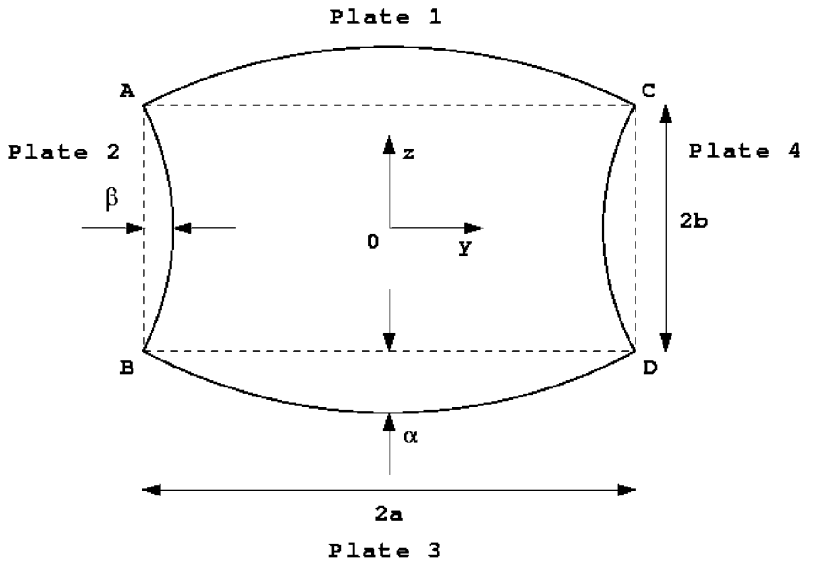

Fig. 6. Cross-section considered motion for the approximate analytical theory.

(Branch number 6 in the dispersion curve given in Fig. 5) is considered here. In view of describing this kind of cross-sectional motion, a parabolic shape motion of each panel is assumed (see Fig. 6). This is a symmetrical motion, in which two variables appear: α and β. The third parameter introduced in this approximation is V. V corresponds to the rigid displacement (translation) of the structure. Henceforth, V_i and W_i can be expressed with the three parameters as follows:

$$\begin{aligned} V_1 &= V \quad \text{and} \quad W_1 = -\frac{\alpha}{a^2}(y^2 - a^2), \\ V_2 &= V - \frac{\beta}{b^2}(z^2 - b^2) \quad \text{and} \quad W_2 = 0, \\ V_3 &= V \quad \text{and} \quad W_3 = \frac{\alpha}{a^2}(y^2 - a^2), \\ V_4 &= V + \frac{\beta}{b^2}(z^2 - b^2) \quad \text{and} \quad W_4 = 0. \end{aligned} \tag{34}$$

Moreover, at points A, B, C and D, the right angle is maintained. This leads to the following relationship linking the derivative of V and W. For instance,

$$\frac{\partial W_1}{\partial y}(-a) = \frac{\partial V_2}{\partial z}(-b). \tag{35}$$

So

$$\beta = -\frac{b}{a}\alpha. \tag{36}$$

Concerning the displacement U_i, a further parameter γ is introduced. It is employed in order to consider the flexural motion of the thin-walled structure (see Fig. 7). The complex variable

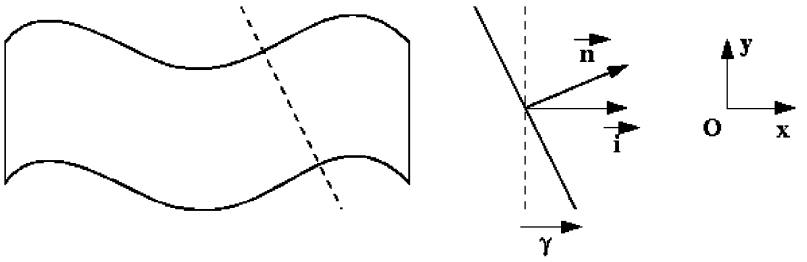

Fig. 7. Significance of the parameter γ.

$(\mathrm{j}, \mathrm{j}^2 = -1)$ is necessary in order to take into account the phase between displacement. Ultimately, the displacement profile approximation can be summarized as follows:

$$\begin{aligned}
&V_1 = V, \quad W_1 = -\frac{\alpha}{a^2}(y^2 - a^2), \quad U_1 = \mathrm{j}U + \mathrm{j}\gamma\,\frac{y}{a},\\
&V_2 = V + \frac{\alpha}{ab}(z^2 - b^2), \quad W_2 = 0, \quad U_2 = \mathrm{j}U + \mathrm{j}\gamma,\\
&V_3 = V, \quad W_3 = \frac{\alpha}{a^2}(y^2 - a^2), \quad U_3 = \mathrm{j}U + \mathrm{j}\gamma\,\frac{y}{a},\\
&V_4 = V - \frac{\alpha}{ab}(z^2 - b^2), \quad W_4 = 0, \quad U_4 = \mathrm{j}U - \mathrm{j}\gamma.
\end{aligned} \tag{37}$$

The usual format of Hamilton's equations for the problem can thus be employed. The generalized displacement quantities U, α, γ and V are considered. The displacement profile given in Eq. (37) is introduced in the kinetic and potential energy expression. In Appendix B, some detailed expressions are given. The results of Hamilton's equations after some mathematics lead to the following system of equations:

$$\begin{aligned}
&\left(\frac{Ek^2}{1-v^2} - \rho\omega^2\right)U = 0,\\
&\left(\tfrac{2}{15}k^4(a^3+b^3) + \tfrac{2}{3}k^2(a+b) + \left(\frac{1}{a}+\frac{1}{b}\right) - \tfrac{8}{5}\rho\omega^2\,\frac{1-v^2}{Eh^2}(a^3+b^3)\right)\alpha = 0,\\
&\left(\frac{E}{1-v^2}\left(k^2\left(\frac{a}{3}+b\right) + \frac{1-v}{2a}\right) - \rho\omega^2\left(\frac{a}{3}+b\right)\right)\gamma + \frac{Ek}{2(1+v)}V = 0,\\
&\frac{Ek}{2(1-v)}\gamma + \left(\frac{Eh^2bk^4}{12(1-v^2)} + \frac{Eak^2}{2(1-v)} - \rho\omega^2(a+b)\right)V = 0.
\end{aligned} \tag{38}$$

System (38) can be put in a more convenient format:

$$\begin{pmatrix} a_{11} & 0 & 0 & 0\\ 0 & a_{22} & 0 & 0\\ 0 & 0 & a_{33} & a_{34}\\ 0 & 0 & a_{43} & a_{44} \end{pmatrix}\begin{pmatrix} U\\ \alpha\\ \gamma\\ V \end{pmatrix} = \begin{pmatrix} 0\\ 0\\ 0\\ 0 \end{pmatrix}. \tag{39}$$

The solutions of such a system can be reached for a singular matrix. This leads to three solutions corresponding simply to: $a_{11}=0$, $a_{22}=0$ and $a_{33}a_{44}-a_{34}a_{43}=0$. Precisely,

- a traction mode corresponding to $a_{11}=0$ and leading to

$$k=\omega\sqrt{\frac{\rho(1-\nu^2)}{E}}, \tag{40}$$

- a flexural mode corresponding to $a_{33}a_{44}-a_{34}a_{43}=0$:

$$\begin{aligned}&\frac{E^2h^2}{12(1-\nu^2)^2}\,b\left(\frac{a}{3}+b\right)k^6+\left(\frac{E^2}{2(1-\nu)(1+\nu)^2}\,a\left(\frac{a}{3}+b\right)+\frac{E^2h^2}{24(1-\nu)(1+\nu)^2}\,\frac{a}{b}\right.\\&\left.-\frac{Eh^2}{12(1-\nu^2)}\,\rho\omega^2 b\left(\frac{a}{3}+b\right)\right)k^4-\frac{E}{1+\nu}\,\rho\omega^2\left(\frac{a}{3}+b\right)\left(\frac{a}{2}+\frac{a+b}{1-\nu}\right)k^2\\&+\rho^2\omega^4(a+b)\left(\frac{a}{3}+b\right)-\frac{E}{2(1+\nu)}\rho\omega^2\,\frac{a+b}{a}=0.\end{aligned} \tag{41}$$

This equation is solved here using Cardan's formulae.

- a cross-section mode corresponding to $a_{22}=0$:
  If $\omega>\omega_c$,

$$k=\sqrt{\frac{-\frac{2}{3}(a+b)+\sqrt{\Delta}}{\frac{4}{15}(a^3+b^3)}}$$

  with

$$\omega_c=\frac{5}{8}\,\frac{Eh^2}{\rho(1-\nu^2)}\,\frac{1}{a^3+b^3}\left(\frac{1}{a}+\frac{1}{b}\right)$$

  and

$$\Delta=\tfrac{4}{9}(a+b)^2-\tfrac{8}{15}(a^3+b^3)\left(\left(\frac{1}{a}+\frac{1}{b}\right)-\tfrac{8}{5}\rho\omega^2\,\frac{(1-\nu^2)}{Eh^2}(a^3+b^3)\right). \tag{42}$$

In the next subsection, the analytical theory presented is compared with a full numerical processing of the dispersion curve extraction procedure.

4.2.3. Comparisons and comments

Fig. 8 presents a comparison between the dispersion curves obtained from three different approaches. The first approach is the classical beam theory considering both flexural motion as well as compressional motion. The second theory (designated by plate assembly in the given figure) is the one presented previously, whilst the last theory (designated in this figure by present) represents the numerical extraction procedure proposed in this paper. It should be noted that, for

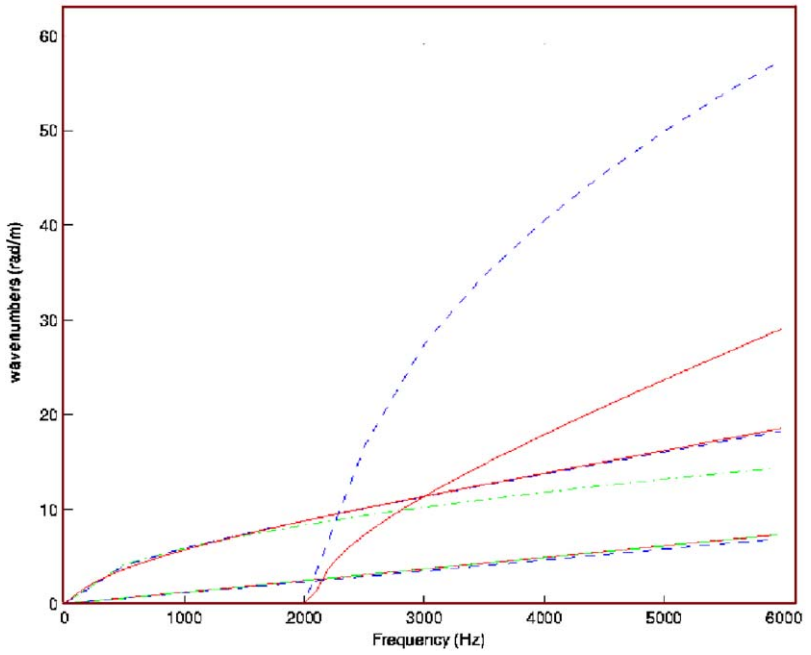

Fig. 8. Comparison of dispersion curves associated to considered theories: dash–dot, Euler–Bernoulli; dashed, plate assembly; solid, present method.

the sake of clarity, only the pumping mode is represented in this figure. Fig. 4 from the FEM interface presents the full extracted propagation constant associated with the plate box structure within the frequency band [0 Hz; 6000 Hz].

From the dispersion curve synthesis given in Fig. 8, it can be remarked that both the plate assembly approach and the numerical procedure (present—Eq. (25)) predict a similar frequency evolution of the flexural and the longitudinal waves. The cut-on frequency is predicted correctly by the plate assembly analytical theory when compared with the numerical procedure. However, as mentioned in the cylinder case study, the amplitude of the predicted wavenumber differs in the two theories. This is mainly due to the fact that the pumping mode is not fully described by the analytical theory. In fact, it seems that the parabolic approximation is not sufficient, especially as the frequency increases. A more concise approximate theory can thus be proposed using a higher interpolation order for the motion of the plate box structure. This will obviously lead to less analytical simplicity than expected. This conclusion proves the interest of a numerical hybridization of the dispersion extraction procedure.

5. Full automotive frame numerical study

The main objective of this section is to validate the present approach for a full-scale realistic thin-walled structure and to perform a numerical study in view of better understanding

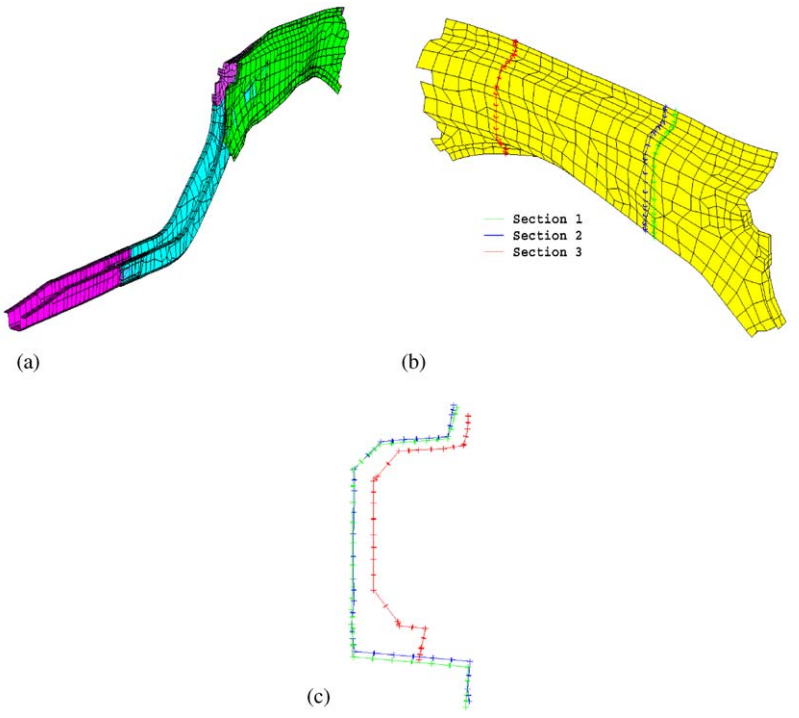

Fig. 9. (a) Full subframe segment finite element model; (b) the front subframe segment under consideration; (c) three considered sections for the dispersion curves extraction.

the wave transfer mechanism for such realistic cases. A numerical study is then proposed in order to see the influence of the length of the considered structure and the wave contents. The structure considered is a realistic piece of rail taken from an existing full automotive finite element model.

5.1. Analysis of an automotive subframe segment

In the automotive industry, passive security remains an important and strategic issue. Mastering the dissipated energy and understanding the propagation mechanism at impact, for instance, can be of fundamental importance and play a leading role in the design of optimized structures. The structure considered here is extracted from a full-scale finite element model of an automobile: a subframe segment (see Fig. 9). It is a typical structure, which carries the engine. The main solid-borne energy is thus propagated through such a structure and generates vibration and radiated sound. The structure under consideration consists of two main parts. Here, the wave behaviour of the front part of the subframe (see Fig. 9) is analysed. The front subframe length is approximately 55 cm, made from a HLE275D steel ($E = 2.068 \times 10^{11}\,\mathrm{N/m^2}$, $\nu = 0.29$ and $\rho = 7850\,\mathrm{kg/m^3}$). Its thickness is 1.76 mm. Three sections of different topologies were considered. These sections are shown in Fig. 9.

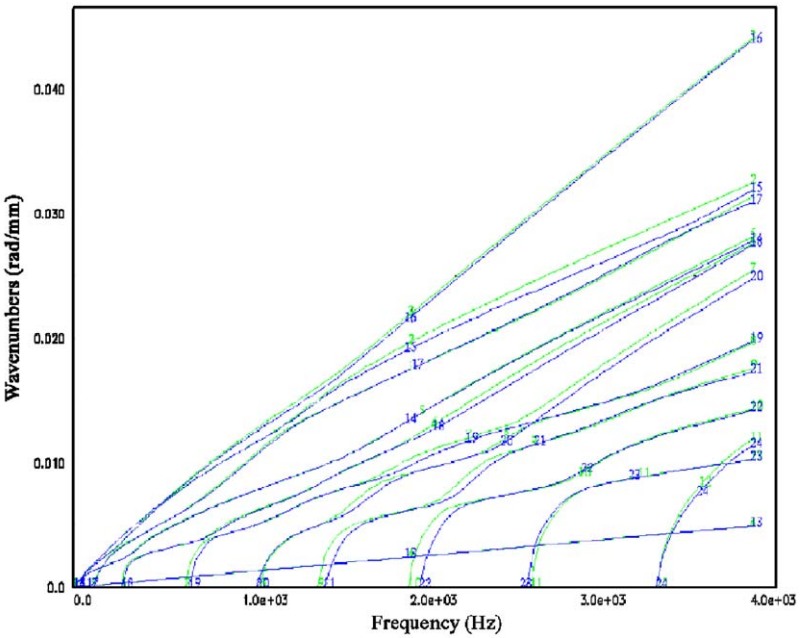

Fig. 10. Dispersion curve comparison: sections 1 and 2 of the front subframe segment.

5.2. *Wave motion of the automobile subframe segment*

For all these sections, the average nodal distance is 15 mm. Using FEM code, a mesh of this piece was generated with a propagation distance d equal to 20 mm. The frequency step used is 40 Hz and 100 frequencies were chosen. Fig. 10 provides dispersion curve comparisons associated to sections 1 and 2, whilst Fig. 11 provides those concerning sections 1 and 3. It can be seen in Fig. 9 that sections 1 and 2 are geometrically close, but differ in the number of nodes in each section. It is interesting to note that similar dispersion curves are obtained (see Fig. 10). Indeed, equal propagation branches and close cut-on frequencies can be observed. In contrast, the propagation features associated to sections 1 and 3 are divergent (see Fig. 11), whereas the deformed shapes associated to different modes are given in Fig. 12. Twelve propagation branches are extracted for section 1, whilst only ten branches appear for section 3. Moreover, a comparison of cut-on frequencies shows notable discrepancies. This is mainly due to the topological differences between sections 1 and 3; indeed, the uniform cross-section is needed in the dispersion curve extraction technique proposed here. Further developments should be made in order to extend the formulation to non-uniform geometries. Ultimately, this example demonstrates that the propagation constants and the associated physics can be affected drastically by the design of such thin-walled structures. In fact, one can control the wave characteristics, number and nature by correctly designing the structures. It thus becomes possible to imagine structures, in the early stage of design, with high vibratory and acoustics performance with a kind of *wave trap*.

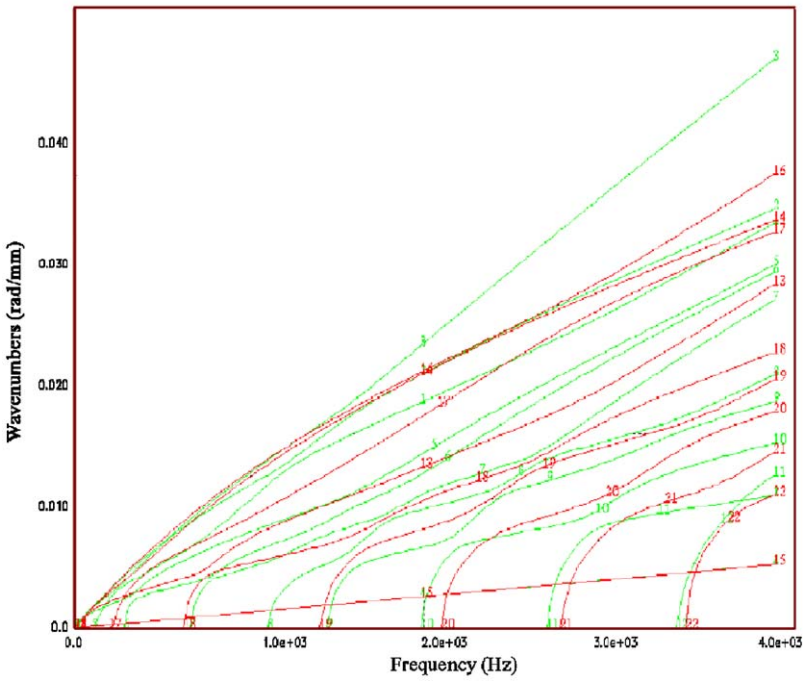

Fig. 11. Dispersion curve comparison: sections 1 and 3 of the front subframe segment.

6. Conclusion

In this paper, the wave motion of thin-walled structures was studied. A numerical procedure was proposed in order to extract propagation parameters of any cross-section thin-walled structure. The procedure was also implemented under a finite element code leading to an effective tool for analysing the free waves of realistic situations.

Many comments and conclusions can be drawn from the developments presented in this contribution. It has been clearly shown that analytical theories are of limited value, particularly at high frequencies. Indeed, the 3D behaviour is required in such frequency ranges and the results of some analytical theories have proved to be limited due to the employed assumptions. The numerical procedure employed can provide important data for predictive high-frequency tools, mainly SEA [13] and its local format. Waves extracted from this numerical analysis can also be employed in view of a forced response study and consideration.

Moreover, from a free wave analysis, one can imagine some interesting optimization solutions at preliminary steps in the product life. Hence, with appropriate modifications in the geometrical as well as mechanical properties of the structures, one can control waves carrying most of the energy or generating excessive sound. Generalization of the procedure is under progress. Indeed, the formulation established here can be reached from a more theoretical work on an elastoacoustic dissipative medium with or without sound radiation. The introduction of a damping mechanism affects notably the formulation presented here and leads to intrinsic considerations and numerical artifice in order to simplify the obtained spectral formulation.

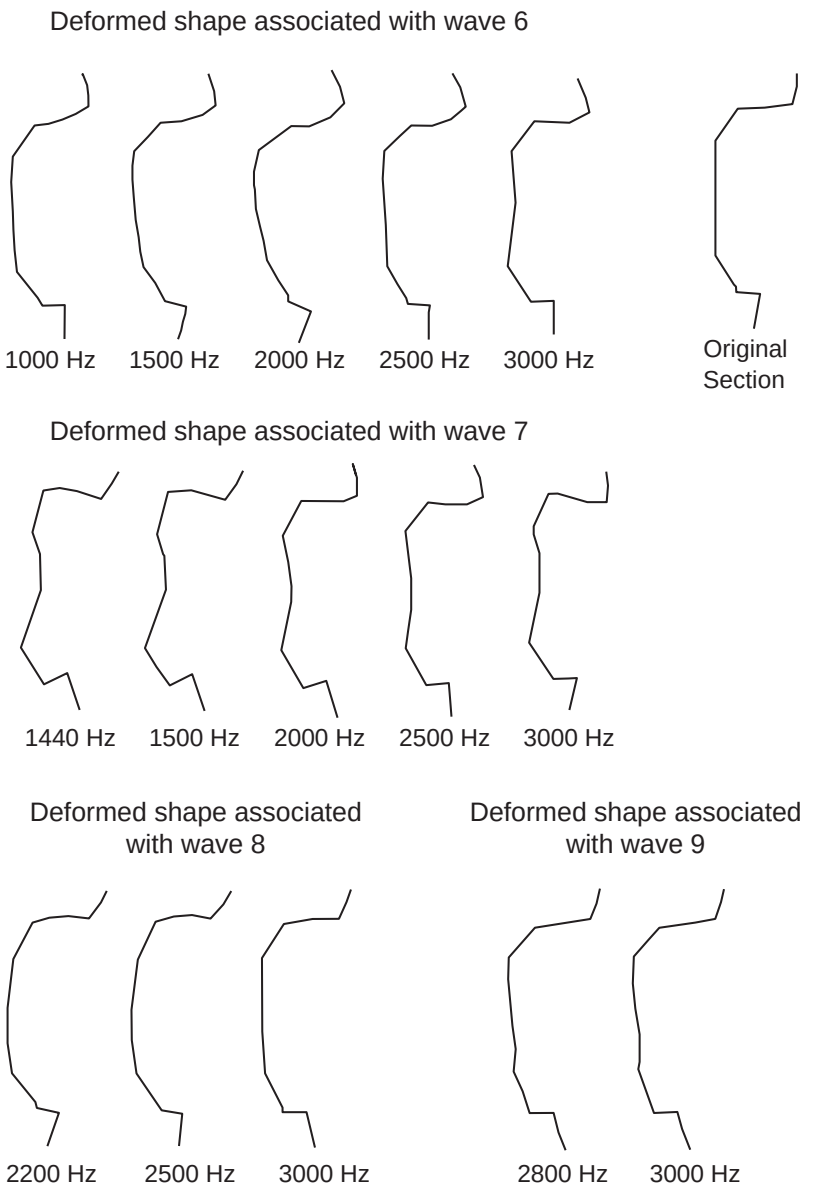

Fig. 12. Deformed shapes: cross-section 3 associated with propagation branches 6–9.

Acknowledgements

The authors gratefully acknowledge Mr B. Hazet (PSA Velizy) for his scientific collaboration, his advice and encouragement. We owe our thanks to Miss R. Reynaud for English assistance and to reviewers for their valuable comments.

Appendix A

Potential energy expressions for plate box structures are as follows:

- *For plate* 1:

$$Ep_1 = \frac{1}{2}\frac{Eh}{1-v^2} L \int_{-a}^{a} \left(k^2 U_1 \overline{U_1} + \frac{\partial V_1}{\partial y}\frac{\partial \overline{V_1}}{\partial y} + v\left(-\mathrm{j}k\overline{U_1}\frac{\partial V_1}{\partial y} + \mathrm{j}kU_1\frac{\partial \overline{V_1}}{\partial y}\right) + \frac{1-v}{2}\left(\frac{\partial \overline{U_1}}{\partial y} - \mathrm{j}k\overline{V_1}\right)\left(\frac{\partial U_1}{\partial y} + \mathrm{j}kV_1\right)\right) \mathrm{d}y + \frac{Eh^3}{24(1-v^2)} L \int_{-a}^{a} \left(k^4 \overline{W_1} W_1 - vk^2\left(\overline{W_1}\frac{\partial^2 W_1}{\partial y^2} + W_1\frac{\partial^2 \overline{W_1}}{\partial y^2}\right) + \frac{\partial^2 \overline{W_1}}{\partial y^2}\frac{\partial^2 W_1}{\partial y^2} + 2(1-v)k^2\frac{\partial \overline{W_1}}{\partial y}\frac{\partial W_1}{\partial y}\right) \mathrm{d}y.$$

- *For plate* 2:

$$Ep_2 = \frac{1}{2}\frac{Eh}{1-v^2} L \int_{-b}^{b} \left(k^2 U_2 \overline{U_2} + \frac{\partial W_2}{\partial z}\frac{\partial \overline{W_2}}{\partial z} + v\left(-\mathrm{j}k\overline{U_2}\frac{\partial W_2}{\partial z} + \mathrm{j}kU_2\frac{\partial \overline{W_2}}{\partial z}\right) + \frac{1-v}{2}\left(\frac{\partial \overline{U_2}}{\partial z} - \mathrm{j}k\overline{W_2}\right)\left(\frac{\partial U_2}{\partial z} + \mathrm{j}kW_2\right)\right) \mathrm{d}z + \frac{Eh^3}{24(1-v^2)} L \int_{-b}^{b} \left(k^4 \overline{V_2} V_2 - vk^2\left(\overline{V_2}\frac{\partial^2 V_2}{\partial z^2} + V_2\frac{\partial^2 \overline{V_2}}{\partial z^2}\right) + \frac{\partial^2 \overline{V_2}}{\partial z^2}\frac{\partial^2 V_2}{\partial z^2} + 2(1-v)k^2\frac{\partial \overline{V_2}}{\partial z}\frac{\partial V_2}{\partial z}\right) \mathrm{d}z.$$

- *For plate* 3:

$$Ep_3 = \frac{1}{2}\frac{Eh}{1-v^2} L \int_{-a}^{a} \left(k^2 U_3 \overline{U_3} + \frac{\partial V_3}{\partial y}\frac{\partial \overline{V_3}}{\partial y} + v\left(-\mathrm{j}k\overline{U_3}\frac{\partial V_3}{\partial y} + \mathrm{j}kU_3\frac{\partial \overline{V_3}}{\partial y}\right) + \frac{1-v}{2}\left(\frac{\partial \overline{U_3}}{\partial y} - \mathrm{j}k\overline{V_3}\right)\left(\frac{\partial U_3}{\partial y} + \mathrm{j}kV_3\right)\right) \mathrm{d}y + \frac{Eh^3}{24(1-v^2)} L \int_{-a}^{a} \left(k^4 \overline{W_3} W_3 - vk^2\left(\overline{W_3}\frac{\partial^2 W_3}{\partial y^2} + W_3\frac{\partial^2 \overline{W_3}}{\partial y^2}\right) + \frac{\partial^2 \overline{W_3}}{\partial y^2}\frac{\partial^2 W_3}{\partial y^2} + 2(1-v)k^2\frac{\partial \overline{W_3}}{\partial y}\frac{\partial W_3}{\partial y}\right) \mathrm{d}y.$$

- *For plate* 4:

$$Ep_4 = \frac{1}{2}\frac{Eh}{1-v^2} L \int_{-b}^{b} \left(k^2 U_4 \overline{U_4} + \frac{\partial W_4}{\partial z}\frac{\partial \overline{W_4}}{\partial z} + v\left(-\mathrm{j}k\overline{U_4}\frac{\partial W_4}{\partial z} + \mathrm{j}kU_4\frac{\partial \overline{W_4}}{\partial z}\right) + \frac{1-v}{2}\left(\frac{\partial \overline{U_4}}{\partial z} - \mathrm{j}k\overline{W_4}\right)\left(\frac{\partial U_4}{\partial z} + \mathrm{j}kW_4\right)\right) \mathrm{d}z + \frac{Eh^3}{24(1-v^2)} L \int_{-b}^{b} \left(k^4 \overline{V_4} V_4 - vk^2\left(\overline{V_4}\frac{\partial^2 V_4}{\partial z^2} + V_4\frac{\partial^2 \overline{V_4}}{\partial z^2}\right) + \frac{\partial^2 \overline{V_4}}{\partial z^2}\frac{\partial^2 V_4}{\partial z^2} + 2(1-v)k^2\frac{\partial \overline{V_4}}{\partial z}\frac{\partial V_4}{\partial z}\right) \mathrm{d}z.$$

Appendix B

Potential and kinetic energy details for the approximate plate assembly theory are:

- *For plate* 1:

$$Ec_1 = \frac{1}{2}\rho\omega^2 Lh \int_{-a}^{a} \left(\left(U + \gamma\frac{y}{a}\right)^2 + V^2 + \frac{\alpha^2}{a^4}(y^2-a^2)^2\right) \mathrm{d}y,$$

$$Ep_1 = \frac{1}{2}\frac{Eh}{1-v^2} L \left(\int_{-a}^{a} \left(k^2\left(U + \gamma\frac{y}{a}\right)^2 + \frac{1-v}{2}\left(\frac{\gamma}{a} + kV\right)^2\right) \mathrm{d}y + \frac{h^2}{12}\int_{-a}^{a} \left(k^4\frac{\alpha^2}{a^4}(y^2-a^2)^2 + \frac{4\alpha^2}{a^4} - 4vk^2\frac{\alpha^2}{a^4}(y^2-a^2) + (1-v)k^2\frac{8\alpha^2}{a^4}y^2\right) \mathrm{d}y\right).$$

- *For plate* 2:

$$Ec_2 = \frac{1}{2}\rho\omega^2 Lh \int_{-b}^{b} \left((U+\gamma)^2 + \left(V + \frac{\alpha}{ab}(z^2-b^2)\right)^2\right) \mathrm{d}z,$$

$$Ep_2 = \frac{1}{2}\frac{Eh}{1-v^2} L \left(\int_{-b}^{b} k^2(U+\gamma)^2\,\mathrm{d}z + \frac{h^2}{12}\int_{-b}^{b} \left(k^4\left(V + \frac{\alpha}{ab}(z^2-b^2)\right)^2 + \frac{4\alpha^2}{a^2b^2} - 4\frac{\alpha v}{ab}k^2\left(V + \frac{\alpha}{ab}(z^2-b^2)\right) + (1-v)k^2\frac{8\alpha^2}{a^2b^2}z^2\right) \mathrm{d}z\right).$$

- *For plate* 3:

$$Ec_3 = \frac{1}{2}\rho\omega^2 Lh \int_{-a}^{a} \left(\left(U + \gamma\frac{y}{a}\right)^2 + V^2 + \frac{\alpha^2}{a^4}(y^2-a^2)^2\right) \mathrm{d}y,$$

$$Ep_3 = \frac{1}{2}\frac{Eh}{1-v^2} L \left(\int_{-a}^{a} \left(k^2\left(U + \gamma\frac{y}{a}\right)^2 + \frac{1-v}{2}\left(\frac{\gamma}{a} + kV\right)^2\right) \mathrm{d}y + \frac{h^2}{12}\int_{-a}^{a} \left(k^4\frac{\alpha^2}{a^4}(y^2-a^2)^2 + \frac{4\alpha^2}{a^4} - 4vk^2\frac{\alpha^2}{a^4}(y^2-a^2) + (1-v)k^2\frac{8\alpha^2}{a^4}y^2\right) \mathrm{d}y\right).$$

- *For plate* 4:

$$Ec_4 = \frac{1}{2}\rho\omega^2 Lh \int_{-b}^{b}\left((U-\gamma)^2 + \left(V - \frac{\alpha}{ab}(z^2-b^2)\right)^2\right)\mathrm{d}z,$$

$$Ep_4 = \frac{1}{2}\frac{Eh}{1-v^2} L\left(\int_{-b}^{b} k^2(U-\gamma)^2\,\mathrm{d}z + \frac{h^2}{12}\int_{-b}^{b}\left(k^4\left(V - \frac{\alpha}{ab}(z^2-b^2)\right)^2 + \frac{4\alpha^2}{a^2b^2} + 4\frac{\alpha v}{ab}k^2\left(V - \frac{\alpha}{ab}(z^2-b^2)\right) + (1-v)k^2\frac{8\alpha^2}{a^2b^2}z^2\right)\mathrm{d}z\right).$$

References

[1] L. Cremer, M. Heckl, E.E. Ungar, *Structure-borne Sound*, Springer, Berlin, 1988.
[2] K.U. Morse, H. Feshbach, *Methods of Theoretical Physics*, McGraw Hill, New York, 1953.
[3] G. Dhatt, J.L. Batoz, *Modélisation des Structures par Éléments Finis*, Hermes, Paris, 1992.
[4] R.H. Lyon, *Statistical Energy Analysis of Dynamical Systems: Theory and Application*, MIT Press, Cambridge, MA, 1975.
[5] A.J. Keane, W.G. Price, *Statistical Energy Analysis: An Overview, With Applications in Structural Dynamics*, Cambridge University Press, Cambridge, 1997.
[6] F.J. Fahy, L'analyse statistique énergétique, *Revue d'Acoustique* 33 (1975).
[7] F.J. Fahy, Statistical energy analysis: a critical overview, *Philosophical Transaction of the Royal Society of London A* 346 (1994).
[8] D.J. Nefske, S.H. Sung, Power flow finite element analysis of dynamic systems: basic theory and application to beams, *NCA Publication* 3 (1987).
[9] J.C. Wohlever, R.J. Bernhard, Mechanical energy flow models of rods and beams, *Journal of Sound and Vibration* 153 (1992) 1–19.
[10] Y. Lase, M.N. Ichchou, L. Jezequel, Energy analysis of bars and beams: theoretical formulations, *Journal of Sound and Vibration* 192 (1996) 281–305.
[11] M.N. Ichchou, L. Jezequel, Comments on simple models of the energy flow in vibrating membranes and transversely vibrating plates, *Journal of Sound and Vibration* 195 (1996) 679–685.
[12] M.N. Ichchou, A. Le Bot, L. Jezequel, Energy models of one-dimensional multi-propagative systems, *Journal of Sound and Vibration* 201 (1997) 535–554.
[13] S. Finnveden, Evaluation of modal density and group velocity by a finite element method, *Journal of Sound and Vibration* 273 (1–2) (2004) 51–57.
[14] L. Gavric, Computation of propagatives waves in free rail using a finite element technique, *Journal of Sound and Vibration* 185 (3) (1995) 531–543.
[15] L. Gavric, Finite element computation of dispersion properties of thin walled waveguides, *Journal of Sound and Vibration* 173 (1) (1994) 113–124.
[16] K. Knothe, Z. Strzyzakowski, K. Willner, Rail vibrations in the high frequency range, *Journal of Sound and Vibration* 169 (1) (1994) 111–123.
[17] Y.K. Lin, B.K. Donaldson, A brief survey of transfer matrix techniques with special reference to the analysis of aircraft panels, *Journal of Sound and Vibration* 10 (1) (1969) 103–143.
[18] D.J. Mead, A general theory of harmonic wave propagation in linear periodic systems with multiple coupling, *Journal of Sound and Vibration* 27 (2) (1973) 235–260.
[19] D.J. Mead, Wave propagation and natural modes in periodic systems: multi-coupled systems, with and without damping, *Journal of Sound and Vibration* 40 (1) (1975) 19–39.
[20] P.H. Denke, G.R. Eide, J. Pickard, Matrix difference equation analysis of vibrating periodic structures, *AIAA Journal* 13 (2) (1974) 160.

[21] D.J. Thompson, Wheel-rail noise generation—part iv: contact zone and results, *Journal of Sound and Vibration* 161 (3) (1993) 447–466.
[22] W.X. Zhong, F.W. Williams, On the direct solution of wave propagation for repetitive structures, *Journal of Sound and Vibration* 181 (3) (1995) 485–501.
[23] W. Zhong, X. Zhong, On the adjoint simplectic inverse substitution method for main eigensolutions of a large hamitonian matrix, *Journal of System Engineering* 1 (1991) 41–50.
[24] S. Finnveden, Spectral finite element analysis of the vibration of straight fluid-filled pipes with flanges, *Journal of Sound and Vibration* 199 (1) (1997) 125–154.
[25] S. Finnveden, Formulas for modal density and for input power for mechanical and fluid point sources in fluid filled pipes, *Journal of Sound and Vibration* 208 (5) (1997) 705.
[26] M.N. Ichchou, Formulations Énergétiques pour l'Étude Moyennes et Hautes Fréquences des Systèmes: Théorie et Application, PhD Thesis, Ecole Centrale de Lyon, 1996 (numero 96-ECDL-10).
[27] A. Bocquillet, Méthode Énergétique de Caractérisations Vibroacoustiques des Réseaux Complexes, PhD Thesis, Ecole Centrale de Lyon, février 2000.
[28] L. Houillon, Modélisation Vibratoires des Carrosseries Automobiles en Moyennes et Hautes Fréquences, PhD Thesis, Ecole Centrale de Lyon, Décembre 1999.
[29] U. Orrenius, S. Finnveden, Calculation of wave propagation in rib-stiffened plate structures, *Journal of Sound and Vibration* 198 (2) (1996) 203–224.
[30] A. Bocquillet, M.N. Ichchou, L. Jezequel, Local energy approach to complex periodic systems, in: *InterNoise'99 Congress*, Ft Lauderdale, USA, December 1999.
[31] A. Bocquillet, M.N. Ichchou, A. Le bot, L. Jezequel, SEA and local energy approach of fluid filled pipes, in: *NOVEM'2000 Congress*, Lyon, France, September 2000.
[32] A. Bocquillet, M.N. Ichchou, L. Jezequel, Energetics of axisymmetric fluid filled pipes up to high frequencies, *Journal of Fluid and Structures* 17 (2003) 491–510.
[33] L. Houillon, M.N. Ichchou, L. Jezequel, Thin walled structures propagation characterisation, in: *InterNoise'2000 Congress*, Nice, France, 27–30 August 2000.
[34] S. Markus, *The Mechanics of Vibrations of Cylindrical Shells*, Elsevier, Amsterdam, 1988.